

Origin of skyrmion lattice phase splitting in Zn-substituted Cu_2OSeO_3

A. Štefanič,^{1,*} S. Moody,² T.J. Hicken,² T.M. Birch,² G. Balakrishnan,¹ S.A. Barnett,³ M. Crisanti,^{1,4} J.S.O. Evans,⁵ S.J.R. Holt,² K.J.A. Franke,² P.D. Hatton,² B.M. Huddart,² M.R. Lees,¹ F.L. Pratt,⁶ C.C. Tang,³ M.N. Wilson,² F. Xiao,^{7,8} and T. Lancaster^{2,†}

¹*University of Warwick, Department of Physics, Coventry, CV4 7AL, United Kingdom*

²*Durham University, Department of Physics, South Road, Durham, DH1 3LE, United Kingdom*

³*Diamond Light Source, Harwell Science and Innovation Campus, Didcot OX11 0DE, United Kingdom*

⁴*Institut Laue-Langevin, Large Scale Structures Group,*

71 avenue des Martyrs CS 20156, 38042, Grenoble, Cedex 9, France

⁵*Department of Chemistry, Durham University, South Road, Durham, DH1 3LE, United Kingdom*

⁶*ISIS Facility, STFC Rutherford Appleton Laboratory,*

Chilton Didcot, Oxfordshire, OX11 0QX, United Kingdom

⁷*Laboratory for Neutron Scattering, Paul Scherrer Institut, CH-5232 Villigen PSI, Switzerland*

⁸*Department of Chemistry and Biochemistry, University of Bern, CH-3012 Bern, Switzerland*

(Dated: July 13, 2018)

We present an investigation into the structural and magnetic properties of Zn-substituted Cu_2OSeO_3 , a system in which the skyrmion lattice (SkL) phase in the magnetic field-temperature phase diagram was previously seen to split as a function of increasing Zn concentration. We find that splitting of the SkL is only observed in polycrystalline samples and reflects the occurrence of several coexisting phases with different Zn content, each distinguished by different magnetic behaviour. No such multiphase behaviour is observed in single crystal samples.

There has been considerable recent interest in the synthesis and understanding of materials hosting topological phases, owing to their exotic physics and potential for applications. Skyrmions are nano-sized, topologically-protected magnetic spin textures, which are promising candidates for energy-efficient, high-density storage devices^{1–3}. Skyrmions are found in a number of systems including MnSi ^{4,5}, $\text{Fe}_{1-x}\text{Co}_x\text{Si}$ ^{6,7}, FeGe ⁸, β -Mn type Co-Zn-Mn alloys⁹, Cu_2OSeO_3 ¹⁰, GaV_4S_8 ¹¹, and GaV_4Se_8 ¹². The discovery of skyrmions in the multiferroic insulator, Cu_2OSeO_3 represents an important milestone, because of the possibility of manipulating them with an external electric field.¹⁰ Despite an intensive search, the number of known skyrmion-hosting materials still remains relatively small, owing to the very specific structural properties (absence of inversion centre) and magnetic properties (ferromagnetism and presence of Dzyaloshinskii-Moriya interactions) needed to promote the formation of magnetic skyrmions. An alternative route to expand the number of skyrmionic materials is to utilise a chemical doping/substitution strategy in known skyrmion-hosting systems. This approach has recently been adopted in Cu_2OSeO_3 , where Zn and Ni doping led to observation of splitting of the skyrmion lattice (SkL) phase into two distinct pockets,¹³ and an expansion of the SkL phase¹⁴ respectively.

Cu_2OSeO_3 crystallises in the non-centrosymmetric cubic $P2_13$ space group. Two crystallographically inequivalent Cu^{2+} cations in trigonal bipyramidal and square pyramidal coordination geometry (designated as Cu^{\parallel} and Cu^{\perp} respectively) are present in a ratio 1 : 3. These have spins $S = 1/2$ pointing in opposite directions forming a ferrimagnetic lattice^{15–17}. Magnetic interactions between spins are mediated through oxygen atoms via ferromagnetic and antiferromagnetic superex-

change interactions^{18,19}. As reported by Wu *et al.*,¹³ the magnetic moment of Cu_2OSeO_3 monotonically decreases with increasing Zn-substitution levels, which they interpret in terms of the site-specific substitution of Cu^{2+} cation at the Cu^{\parallel} site with non-magnetic Zn^{2+} . This is accompanied by a splitting of the SkL phase observed in pristine Cu_2OSeO_3 into two distinct pockets.

In order to understand the effect of substitution and to confirm the origin of the SkL splitting in this system, investigations on high-quality single crystals are essential. We have produced single crystals of Zn-substituted Cu_2OSeO_3 for several substitution levels of Zn, allowing us to compare their behavior to that of high-purity polycrystalline materials. We find that the splitting of the SkL phase reflects the presence of multiple structural phases in polycrystalline samples. In contrast, phase-pure single crystal samples do not show such behaviour.

By utilising the chemical vapour phase transport technique, single crystals of Zn-substituted Cu_2OSeO_3 , with nominal 2, 8, and 12% Zn content, were grown. Energy-dispersive X-ray spectroscopy (EDX), X-ray fluorescence (XRF) and inductively coupled plasma mass spectroscopy (ICP MS) measurements on single crystals revealed the Zn-concentrations given in Table I. We use the average values of Zn substitution (0.5, 1.8 and 2.4%) below.

The single crystal samples were investigated on the high-resolution I19 beamline at the Diamond Light Source. The a lattice parameter, extracted from data collected at the Zr K-edge (17.9976 keV), was found to monotonically increase with increasing Zn substitution levels, as expected when substituting Cu^{2+} with the slightly larger Zn^{2+} cations (with atomic radii of 0.65 Å and 0.68 Å for five coordinate $\text{Cu}^{2+}/\text{Zn}^{2+}$ respectively^{20,21}). A close comparison of the struc-

Nominal	ICP MS	EDX	XRF	Average	Polycrystal
2	0.9	0.52(9)	0.12(1)	0.5	2.0
8	1.9	1.71(4)	1.71(1)	1.8	6.4
12	2.4	2.51(3)	2.26(1)	2.4	10.5

TABLE I: Percentage Zn concentration in $(\text{Cu}_{1-x}\text{Zn}_x)_2\text{OSeO}_3$ single crystals determined by ICP MS, EDX and XRF. Zn concentration in corresponding polycrystalline samples is given in the right-most column.

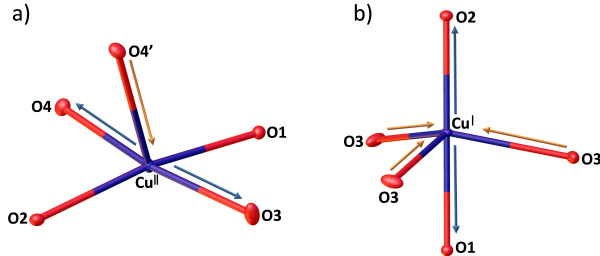


FIG. 1: Structural model for 2.4% Zn-substituted Cu_2OSeO_3 . Coordination environment of (a) the Cu^{II} site (square pyramidal) and (b) the Cu^{I} site (trigonal bipyramidal). Arrows indicate elongation and contraction of bond distances compared to pristine Cu_2OSeO_3 .

tural models for pristine Cu_2OSeO_3 single crystals and 2.4% Zn-substituted Cu_2OSeO_3 revealed a very subtle increase of the short $\text{Cu}^{\text{I}}\text{-O1}$ and $\text{Cu}^{\text{II}}\text{-O2}$ bond distances of 0.004(2) and 0.002(2) Å respectively [Fig. 1]. This leads to an increase of $\text{Cu}^{\text{I}}\text{-Cu}^{\text{II}}$ distances, while the $\text{Cu}^{\text{II}}\text{-Cu}^{\text{II}}$ distances remain the same²².

Polycrystalline materials were synthesised as reported in the Supplemental Material²². The phase-purity and lattice parameters were investigated using high-resolution powder x-ray diffraction (PXRD) at the I11 beamline, Diamond Light Source, with diffraction patterns for each Zn-substituted polycrystalline samples measured at 15.02 keV. A simple axial model was used to describe the peak asymmetry at low angles arising from axial divergence of the beam and a pseudo-Voigt function to describe the Cu_2OSeO_3 peak shapes.

In the unsubstituted material, a single phase of Cu_2OSeO_3 is sufficient to model the diffraction pattern, with small residuals. However, for the samples with increased substitution, all of the peaks in the diffraction pattern split, as shown in Figs. 2(a)-(f). Refinements revealed that this splitting could only be effectively modelled by the inclusion of two or three distinct Cu_2OSeO_3 phases with differing lattice parameters, suggesting that the polycrystalline materials are multiphase under the synthetic conditions used.

Based on our refinements, the lattice parameter a and cell volume of each phase increases monotonically with increasing Zn-substitution levels (Fig. 4), consistent with the behaviour of the single crystals. Using our PXRD measurements, the estimated Zn-substitution levels in

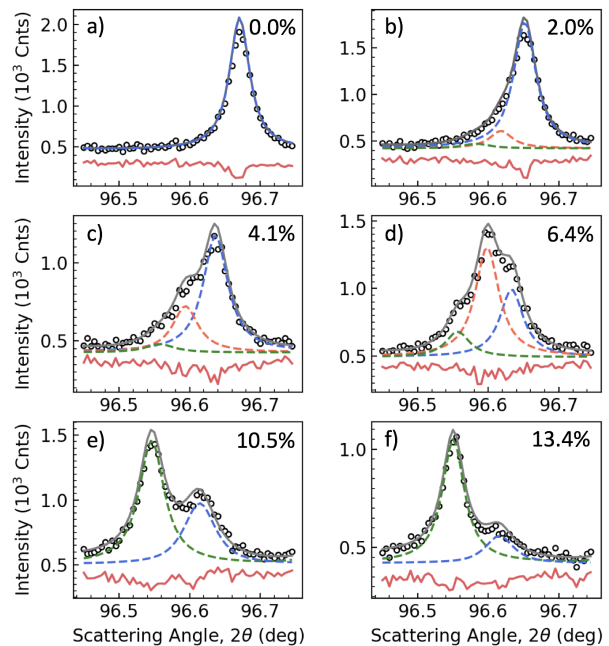


FIG. 2: Left inset: high angle part of the pattern. *Right inset*, showing a single Cu_2OSeO_3 phase is sufficient to model the data. (a)-(f) Powder X-ray diffraction peak at 96.65° for polycrystalline samples with different Zn concentrations, demonstrating that the splitting can be modelled by multiple phases.

polycrystalline samples are taken as 0, 2, 4.1, 6.4, 7.9 10.5 and 13.4%, for the nominal starting compositions of 0, 2, 5, 8, 10, 12 and 15%, respectively.²² The substitution level of Cu^{2+} with Zn^{2+} is higher at low nominal substitution values (up to 5% Zn), while above this level it starts to decrease. This decrease is reflected in the amount of unreacted CuO detected with powder diffraction, increasing from 1% in the sample with 6.4% Zn up to 5% in the sample with 13.4% Zn-substitution level. The crystal structure of Zn_2OSeO_3 , if it exists, is not known, therefore the increase of unreacted CuO with increasing Zn-substitution levels can be related to the stability and Zn^{2+} uptake ability of the Cu_2OSeO_3 crystal structure. In addition, up to 3% of a Zn_2SiO_4 impurity phase was observed in samples with Zn-substitution levels higher than 4%, indicating that ZnO reacts with silica tubes (although we would normally expect this reaction to occur at higher temperatures of $> 1000^\circ\text{C}$ ²³). The estimated Zn concentrations are given in Table I for comparison with the single crystal samples. We note that the Zn uptake is far smaller in the single crystal samples, compared to the polycrystalline analogues.

To characterize the magnetic behavior of all samples, DC magnetic susceptibility measurements were carried out using zero-field-cooled (ZFC) and field-cooled (FC) protocols. Single crystals were aligned with the applied magnetic field directed along the $[111]$ direction. The re-

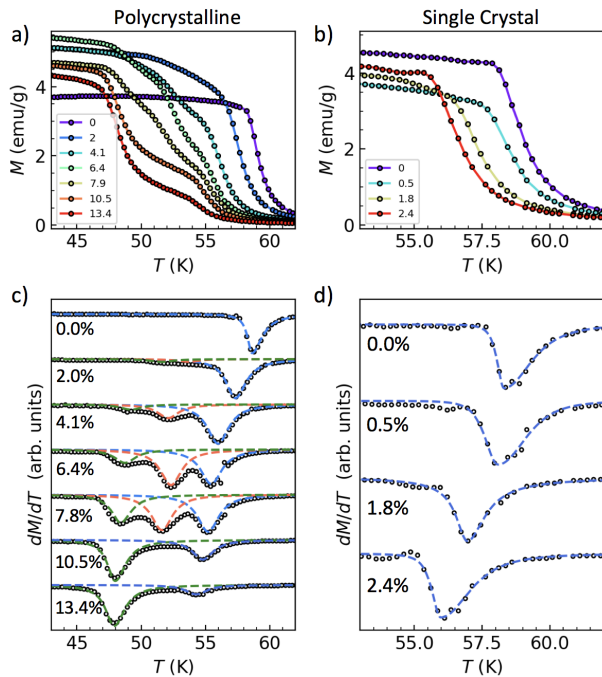


FIG. 3: (a) Magnetization M vs T for polycrystalline samples, measured in a magnetic field of 25 mT. (b) the same for single crystal samples. (c) The derivative of the M vs T polycrystalline data, revealing multiple magnetic transitions. (d) The derivative of the M vs T single crystal data, showing a single transition.

sulting magnetisation curves are shown in Figs. 3(a) and (b). In single crystals the magnetic transition temperature T_c is found to decrease with increasing Zn content. However, the decrease is considerably smaller in single crystals compared to polycrystalline materials, consistent with the relatively low percentage of Zn^{2+} inclusion in the Cu_2OSeO_3 crystal structure. The step-like nature of the data for the polycrystalline material suggests that there are multiple magnetic transitions occurring. This is more clearly seen in the derivative of these data [Fig. 3(c)], which show multiple peaks, particularly for higher Zn substitution, indicating the presence of several magnetic phases with different values of T_c . (This may be contrasted with analogous measurements on single crystals [Fig. 3(d)] showing a single transition.) By fitting the peaks with asymmetric Lorentzian and Split Pearson VII functions for the polycrystalline and single crystal datasets respectively, a critical temperature T_c and volume fraction for each distinct phase was determined, as summarised in Fig. 4.

The existence of skyrmions, along with the size and potential splitting of the skyrmion pocket, were investigated using AC magnetic susceptibility. The resulting magnetic phase diagrams are presented in Fig. 5, where we show the real component χ' as a function of applied field and temperature, which provides a good indication of the

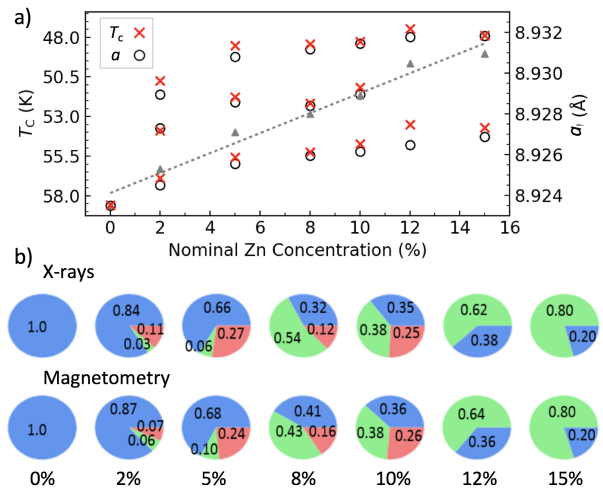


FIG. 4: (a) Critical temperatures T_c (crosses) and lattice parameter a (circles) for each Cu_2OSeO_3 phase in polycrystalline samples, as a function of nominal Zn-substitution. (Triangles show the average lattice parameter a .) (b) Volume fractions of each phase.

helical, conical and skyrmion structures. The phase diagrams for polycrystalline samples closely resemble the data from Wu *et al.*, with T_c of the sample decreasing with increasing Zn substitution, while the skyrmion region seemingly splits into two (or even three in the case of the 6.4% substituted sample) distinct pockets. [This is also seen in the imaginary component of the susceptibility χ''^{22} .] Data measured on single crystals [Fig. 5(e-h)], show a skyrmion phase in each of the samples. The skyrmion pockets in single crystals with 0.5, 1.8 and 2.4% Zn-substitution levels stretch from 54.75 to 57.25 K, 53.5 to 56 K and 52.75 to 55 K respectively. Although the pockets shift to lower temperatures with increasing Zn concentration, their widths remain roughly constant (between 2.25 and 2.5 K), in contrast to the skyrmion pockets detected in polycrystalline materials. The single crystals with 2.4% Zn-substitution level were also measured with $B \parallel$ to $[110]$ and the only noticeable differences are in the shape and size of the skyrmion pocket as reported in the literature²⁴. For $B \parallel$ to $[111]$, the skyrmion pocket can be found in the temperature range between 52.75 and 55.0 K, while for $B \parallel$ $[110]$ the pocket exists from 53.25 to 55.0 K.

Our analysis of the magnetization measurements suggests the presence of multiple magnetic phases in the polycrystalline samples. To establish whether these are intrinsic to the bulk of each material, we carried out longitudinal field (LF) muon-spin relaxation (μSR) measurements, since the muon is a sensitive local probe of bulk magnetism. In order to parametrise the spectra across the measured temperature regime, they were fitted to an exponential function, with the resulting values of relaxation rate λ shown in Fig. 6. We find λ to be significantly

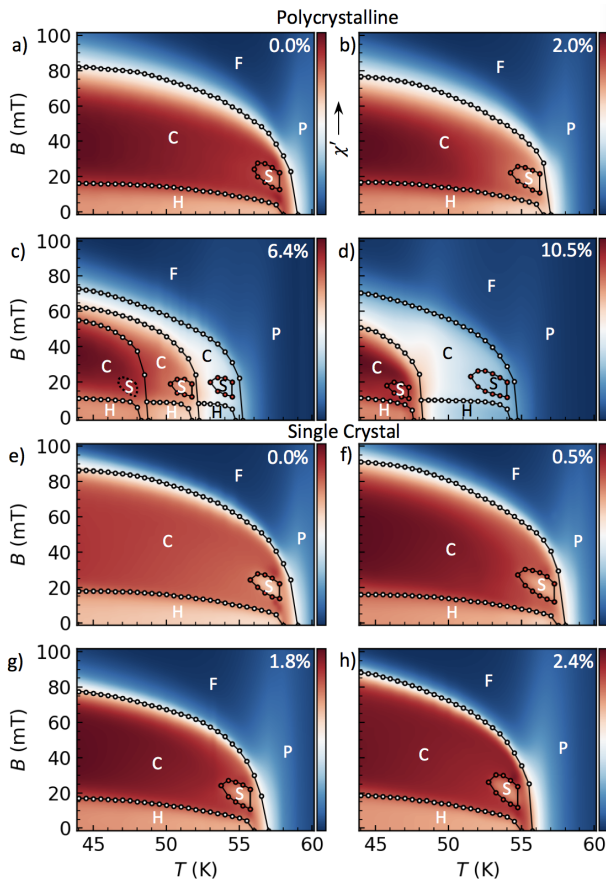


FIG. 5: (a)-(d) Real component of AC susceptibility χ' as a function of field B and temperature T for polycrystalline samples, showing the paramagnetic (P), ferrimagnetic (F), conical (C), helical (H) and skyrmion lattice (S) phases. (e)-(h). The same, but for single crystal samples.

larger inside the SkL phase than outside it. Notably, we observe peaks in λ coinciding with the SkL phases which are significantly broader than the typical peaks that indicate transitions between long-range ordered and paramagnetic phases. This suggests that emergent dynamics in the SkL phase enhance λ . In both 6.4% and 10.5% Zn-substituted materials we see two peaks which coincide with the SkL regions identified above. To estimate the correlation time in the SkL phases, we compared these results and further transverse field μ SR measurements on 6.4% Zn-substituted Cu_2OSeO_3 . From these²⁵ we estimate the correlation time to range between approximately $\tau = 10$ ns at 48 K and $\tau = 70$ ns at 60 K. Within the SkL phase the correlation time increases by almost a factor of two in the lower-temperature SkL phase, and approximately a third in the higher-temperature SkL phase.

Closer examination of the spectra measured for 6.4% Zn substitution near the peaks in λ suggests that they are better described by the sum of two exponential functions with distinct relaxation rates λ_i . This is seen in Fig. 6(a),

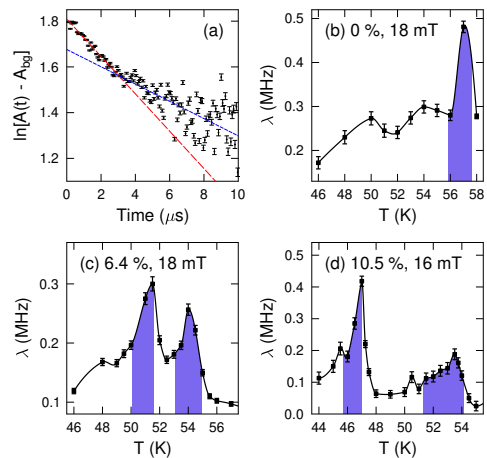


FIG. 6: (a) LF μ SR spectra for 6.4% Zn-substituted Cu_2OSeO_3 measured at 54 K in 18 mT on a logarithmic scale with the background subtracted. Lines are guides to the eye. Relaxation rate λ for LF μ SR measurements of (b) pristine, (c) 6.4% and (d) 10.5% Zn-substituted Cu_2OSeO_3 . Shaded regions indicate the location of the SkL phase derived from AC susceptibility.

where data plotted on a logarithmic scale shows two approximately linear regimes (separated by a crossover at ≈ 2.5 μ s) with significantly different gradients, suggesting that a two-exponential model provides a more accurate description of the data. This strongly implies the occurrence of two magnetically and spatially distinct classes of muon site, with different correlation times, since if there were only one muon site subject to fluctuations with two correlation times, the slower one would dominate, leading to a single relaxation rate²⁶. Moreover, we expect both classes of muon site to occur in the bulk of the material. For comparison, the same analysis was also carried out on LF- μ SR data measured on a polycrystalline sample of pristine Cu_2OSeO_3 (where only one peak is seen). Here, a single exponential function models the data best, suggesting that there is only one magnetically distinct muon site in this material. These measurements therefore provide unambiguous evidence for the coexistence of at least two magnetic phases in the bulk of polycrystalline Zn-substituted Cu_2OSeO_3 .

Evidence for multiple phases in polycrystalline samples has come from structural and magnetic measurements. We may link these with the observation of a correlation between the lattice parameter and T_c for each phase in the polycrystalline samples. These are plotted in Fig. 4(a), labeled by nominal Zn-substitution. The fractional volume of each phase was also determined by both Rietveld refinement and magnetometry and is shown in Fig. 4(b). There is good agreement between the two datasets. We therefore conclude that the polycrystalline Zn-substituted Cu_2OSeO_3 samples are inherently multiphase, featuring multiple, distinct Zn-doped

Cu_2OSeO_3 phases. This then explains the origin of the split skyrmion pocket: each distinct phase exhibits the skyrmion spin structure at a different temperature, reflecting the differing values of T_c .

Although the estimated Zn content in our single crystal samples is, at most, 2.4% and so we might not expect to resolve any splitting in the skyrmion phase, we note that in the 2.0% substituted polycrystalline sample there is evidence for both structural and magnetic phase separation. We see no evidence for multiphase behaviour in our single crystals, suggesting that these are composed of a single phase with a single magnetic transition and should be expected to host a single skyrmion lattice phase.

In conclusion, we have shown that the splitting of

the SkL phase observed exclusively in polycrystalline samples reflects the system's splitting into multiple Zn-substituted phases, each characterized by different magnetic behaviour. This demonstrates the importance of high-quality single crystal samples in the investigation of the magnetic properties of skyrmion hosting systems.

This work is financially supported by EPSRC (EP/N032128/1). Part of this work was performed at the ISIS Facility, Rutherford Appleton Laboratory, Diamond Light Source and the Swiss Muon Source, Paul Scherrer Institut. We are grateful for the provision of beamtime. We thank Matthias Gutmann for useful discussions. Data will be made available via Durham Collections.

* Electronic address: A.Stefancic@warwick.ac.uk

† Electronic address: tom.lancaster@durham.ac.uk

- ¹ J. P. Liu, Z. Zhang, and G. Zhao, *Skyrmions: Topological Structures, Properties, and Applications* (CRC Press, 2016).
- ² N. Nagaosa and Y. Tokura, *Nature Nanotechnology* **8**, 899 (2013).
- ³ A. Fert, V. Cros, and J. Sampaio, *Nature Nanotechnology* **8**, 152 (2013).
- ⁴ S. Mühlbauer, B. Binz, F. Jonietz, C. Pfleiderer, A. Rosch, A. Neubauer, R. Georgii, and P. Böni, *Science* **323**, 915 (2009).
- ⁵ A. Tonomura, X. Yu, K. Yanagisawa, T. Matsuda, Y. Onose, N. Kanazawa, H. S. Park, and Y. Tokura, *Nano Letters* **12**, 1673 (2012).
- ⁶ W. Münzer, A. Neubauer, T. Adams, S. Mühlbauer, C. Franz, F. Jonietz, R. Georgii, P. Böni, B. Pedersen, M. Schmidt, et al., *Physical Review B* **81**, 041203 (2010).
- ⁷ X. Yu, Y. Onose, N. Kanazawa, J. Park, J. Han, Y. Matsui, N. Nagaosa, and Y. Tokura, *Nature* **465**, 901 (2010).
- ⁸ X. Yu, N. Kanazawa, Y. Onose, K. Kimoto, W. Zhang, S. Ishiwata, Y. Matsui, and Y. Tokura, *Nature Materials* **10**, 106 (2011).
- ⁹ Y. Tokunaga, X. Yu, J. White, H. M. Rønnow, D. Morikawa, Y. Taguchi, and Y. Tokura, *Nature Communications* **6**, 7638 (2015).
- ¹⁰ S. Seki, X. Yu, S. Ishiwata, and Y. Tokura, *Science* **336**, 198 (2012).
- ¹¹ I. Kézsmárki, S. Bordács, P. Milde, E. Neuber, L. Eng, J. White, H. M. Rønnow, C. Dewhurst, M. Mochizuki, K. Yanai, et al., *Nature Materials* **14**, 1116 (2015).
- ¹² Y. Fujima, N. Abe, Y. Tokunaga, and T. Arima, *Physical Review B* **95**, 180410 (2017).
- ¹³ H. Wu, T. Wei, K. Chandrasekhar, T. Chen, H. Berger, and H. Yang, *Scientific Reports* **5**, 13579 (2015).
- ¹⁴ K. D. Chandrasekhar, H. Wu, C. Huang, and H. Yang, *Journal of Materials Chemistry C* **4**, 5270 (2016).
- ¹⁵ J.-W. G. Bos, C. V. Colin, and T. T. M Palstra, *Physical Review B* **78**, 094416 (2008).
- ¹⁶ M. Belesi, I. Rousochatzakis, H.C. Wu, H. Berger, I.V. Shvets, F. Mila, and J.-P. Ansermet, *Physical Review B* **82**, 094422 (2010).
- ¹⁷ A. Maisuradze, Z. Guguchia, B. Graneli, H.M. Rønnow, H. Berger, and H. Keller, *Physical Review B* **84**, 064433 (2011).
- ¹⁸ J.-H. Yang, Z.-L. Li, X.Z. Lu, M.-H. Whangbo, S.-H. Wei, X.G. Gong, and H.J Xiang, *Physical Review Letters* **109**, 107203 (2012).
- ¹⁹ I. Živković, D. Pajić, T. Ivek, and H. Berger, *Physical Review B* **85**, 224402 (2012).
- ²⁰ H. Effenberger and F. Pertlik, *Monatshefte für Chemie/Chemical Monthly* **117**, 887 (1986).
- ²¹ R. D. Shannon, *Acta Crystallographica Section A* **32**, 751 (1976).
- ²² Supplemental material contains details of experimental methods, structural parameters and further results of characterization from magnetometry and analysis of the μSR data.
- ²³ E. Bunting, *Journal of the American Ceramic Society* **13**, 5 (1930).
- ²⁴ T. Adams, A. Chacon, M. Wagner, A. Bauer, G. Brandl, B. Pedersen, H. Berger, P. Lemmens, and C. Pfleiderer, *Physical Review Letters* **108**, 237204 (2012).
- ²⁵ A. Yaouanc and P. D. De Reotier, *Muon spin rotation, relaxation, and resonance: applications to condensed matter* (OUP, Oxford, 2011).
- ²⁶ R.H. Heffner, J.E. Sonier, D.E. MacLaughlin, G.J. Nieuwenhuys, G. Ehlers, F. Mezei, S.-W. Cheong, J.S. Gardner, and H. Röder, *Phys. Rev. Lett.* **85**, 3285 (2000).

Supplemental material for Origin of skyrmion lattice phase splitting in Zn-substituted Cu_2OSeO_3

A. Štefančič,^{1,*} S. Moody,² T.J. Hicken,² T.M. Birch,² G. Balakrishnan,¹ S. Barnett,³ M. Crisanti,^{1,4} J.S.O. Evans,⁵ S.J.R. Holt,² K.J.A. Franke,^{2,2} P.D. Hatton,^{2,2} B.M. Huddart,^{2,2} M.R. Lees,¹ F.L. Pratt,⁶ C.C. Tang,³ M.N. Wilson,² F. Xiao,^{7,8} and T. Lancaster^{2,†}

¹University of Warwick, Department of Physics, Coventry, CV4 7AL, United Kingdom

²Durham University, Department of Physics, South Road, Durham, DH1 3LE, United Kingdom

³Diamond Light Source, Harwell Science and Innovation Campus, Didcot OX11 0DE, United Kingdom

⁴Institut Laue-Langevin, Large Scale Structures Group,

71 avenue des Martyrs CS 20156, 38042, Grenoble, Cedex 9, France

⁵Department of Chemistry, Durham University, South Road, Durham, DH1 3LE, United Kingdom

⁶ISIS Facility, STFC Rutherford Appleton Laboratory,

Chilton Didcot, Oxfordshire, OX11 0QX, United Kingdom

⁷Laboratory for Neutron Scattering, Paul Scherrer Institut, CH-5232 Villigen PSI, Switzerland

⁸Department of Chemistry and Biochemistry, University of Bern, CH-3012 Bern, Switzerland

I. SAMPLE PREPARATION

Polycrystalline Cu_2OSeO_3 materials with nominal Zn substitution values of 0, 2, 5, 8, 10, 12 and 15% were synthesised by thoroughly grinding together stoichiometric amounts of CuO (99.99%, metals basis, Alfa Aesar), SeO_2 (99.999%, trace metal basis, Acros Organics) and ZnO (99.999%, Aldrich) inside an argon-filled glove box. The mixtures of powders were transferred into silica tubes, evacuated and sealed. The samples were heated at a rate of $3.5\text{ }^\circ\text{C h}^{-1}$ to $650\text{ }^\circ\text{C}$, kept at this temperature for 96 h, followed by water quench cooling.

Single crystals of Cu_2OSeO_3 with nominal 0, 2, 8 and 12% Zn substitution levels were grown by the chemical vapour phase transport (CVT) technique. Polycrystalline materials (2.5 g), described above, and ≈ 1.5 to 2 mg/cc of the transporting agent, TeCl_4 , were sealed in evacuated silica tubes. The growth of single crystals with Zn substitution levels between 0 and 2.4% was achieved by heating the source part of the tube to $640\text{ }^\circ\text{C}$ and the sink part to $550\text{ }^\circ\text{C}$ for four weeks. Dark olive-green, almost black, single crystals of size $\approx 3 \times 3 \times 3\text{ mm}^3$ (see Fig. S1) were obtained.

II. X-RAY MEASUREMENTS

In-depth structural investigations of polycrystalline samples was carried out at Diamond Light Source (Harwell Science & Innovation Campus) using the high-resolution 3-circle diffractometer, I11 beamline, operating in transmission mode equipped with 5 multi-analysing crystals (MAC) detector. Data was collected at a wavelength of $0.825251(10)\text{ \AA}$, in a 2θ range between 0 and 150° . Rietveld refinements were carried out in TOPAS academic v6.0 software¹.

The single crystal X-ray diffraction was performed on a Fluid Film Devices 3-circle diffractometer using a Dectris Pilatus 2M detector at the I19 beamline, Diamond Light Source (Harwell Science & Innovation Campus)².

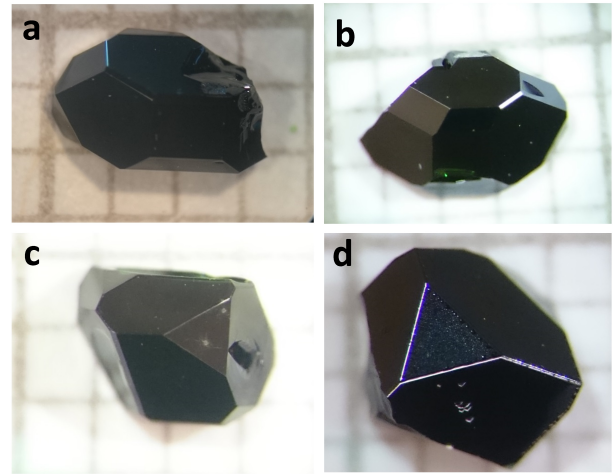


FIG. S1: Single crystals of Cu_2OSeO_3 with (a) 0, (b) 0.5, (c) 1.8, and (d) 2.4% Zn substitution levels respectively. Pictures were taken on millimetre paper.

Data collection at an energy of 17.9976 keV was carried out on 20 to $30\text{ }\mu\text{m}$ size crystals, cleaved from the single crystals shown in Fig. S1.

The xia2³ and DIALS⁴ packages were used for data collection and reduction, and absorption corrections were performed by numerical integration using the SADABS software⁵. Crystal structures were solved by a direct method and refined by full-matrix least squares on F^2 for all data using SHELXT⁶ and SHELXL⁷ embedded in Olex²⁸ software.

The structural model of Cu_2OSeO_3 ⁹, cubic $P2_13$ space group, was refined to diffraction profiles of polycrystalline samples. Results from the synchrotron measurements are given in Table S1. (We also performed laboratory XRD measurements and found that their resolution is insufficient to observe the splitting of the diffraction peaks.) Selected bond lengths and bond angles for single crystal

samples are collected in Tables S2 and S3 respectively.

III. MAGNETIZATION

A Quantum Design Magnetic Property Measurement System, MPMS-5S, superconducting quantum interference device (SQUID) magnetometer was used for investigation of the magnetic properties of the polycrystalline samples and oriented single crystals as a function of temperature and field. Temperature-dependent DC magnetic susceptibility (χ) measurements were carried out in an applied field of 250 Oe in the temperature region between 5 and 110 K under both zero-field-cooled (ZFC) and field-cooled (FC) protocols. AC (χ' and χ'') measurements in an AC driving field of 3 Oe were measured at fixed temperature as a function of DC bias field between 0 and 1000 Oe in order to construct the field (B) *vs* temperature (T) phase diagrams. We assigned the phase boundary of the helical state and the conical state by a sharp increase in the AC susceptibility. The signature of the skyrmion state in these measurements was a sharp drop in the AC susceptibility within the conical phase. Single crystals used for the AC measurements were aligned with $B \parallel$ to $[111]$, with alignment achieved using a Photonic Science X-ray Laue back-scattering imaging system. Ordering temperatures found from the derivatives of the magnetization are given in Tables S4 and S5. The imaginary part χ'' of the AC susceptibility is shown for polycrystalline and single crystal materials in Fig. S2.

IV. MUON-SPIN RELAXATION

In a muon-spin relaxation (μ SR) experiment,¹¹ spin-polarized positive muons are implanted into the sample and subsequently decay into a positron, emitted preferentially in the direction of the muon's instantaneous spin vector. The measured quantity is the time-dependent positron asymmetry $A(t)$, which is proportional to the muon ensemble's spin polarization. Longitudinal field (LF) μ SR measurements (where an external field B_0 is applied parallel to the initial muon-spin direction) were carried out on polycrystalline samples of Cu_2OSeO_3 of 0%, 6.4% and 10.5% Zn-substitution on the HiFi instrument at the ISIS Neutron and Muon Source, Rutherford Appleton Laboratory, UK. Transverse-field (TF) μ SR measurements (applied field perpendicular to the initial spin direction) were made on the 6.4% Zn-substituted Cu_2OSeO_3 using the GPS instrument at the Swiss Muon Source ($S\mu S$), Paul Scherrer Institut, Switzerland. In all cases the samples were packed in silver foil envelopes (foil thickness 12.5 μm) and mounted on a silver plate. For all measurements, samples were zero-field cooled to the minimum temperature, before the field was applied and measurements were made on warming.

In addition to the LF- μ SR measurements described in the main text, measurements were made at fields outside

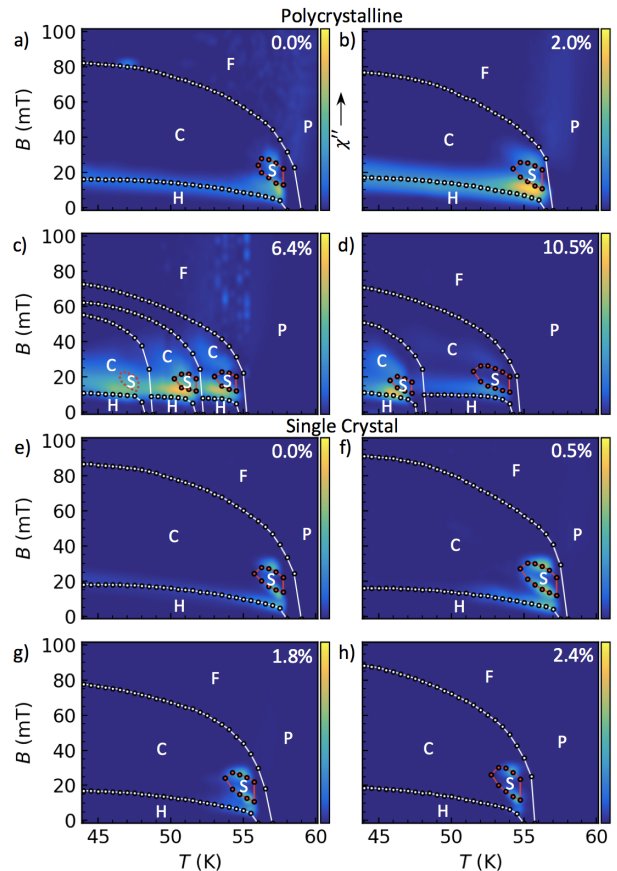


FIG. S2: Imaginary part χ'' of the AC susceptibility for polycrystalline (left column) and single crystal (right column) materials.

the SkL phases. For 6.4% Zn-doped Cu_2OSeO_3 these fields were $B_0 = 5\text{mT}$ (below the minimum field at which the SkL is realized) and 35mT (above the maximum field at which the SkL is realized), whereas for 10.5% Zn-doped Cu_2OSeO_3 a field of 4mT was applied. Spectra for 6.4% Zn-doped Cu_2OSeO_3 were found to relax monotonically and were fitted with a single exponential decay

$$A(t) = A_1 e^{-\lambda t} + A_{\text{bg}}, \quad (1)$$

where the non-relaxing background A_{bg} results from spins that do not relax over the timescale of the measurement, such as those that implant within the Ag foil or sample holder. The extracted values of the longitudinal relaxation rate λ are shown in Fig. S3(a). Note that these peaks appear much sharper than the peaks when cutting through the SkL, as seen in the main text. This shows that cutting through the skyrmion lattice causes an enhanced λ when compared to just cutting through the phase transition.

In the 10.5% Zn-doped Cu_2OSeO_3 data an oscillation

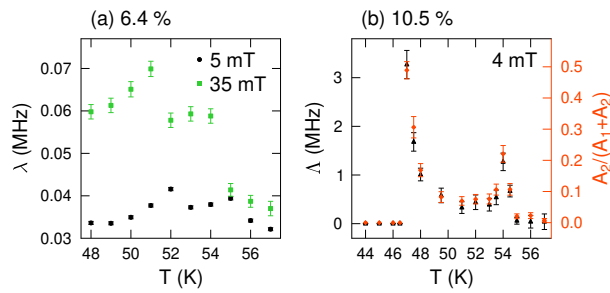


FIG. S3: (a) Relaxation rates for 6.4% Zn-doped Cu_2OSeO_3 at two different applied fields, extracted using fits to Eqn. 1. (b) Transverse relaxation rate Λ and amplitude of oscillating component (both from Eqn. 2) for 10.5% Zn-doped Cu_2OSeO_3 in an applied field of 4 mT.

was observed for $T > 47\text{K}$ (due to spins precessing in

the sum of the applied and internal fields within the ISIS time window). To account for this, these data were fitted to the function

$$A(t) = A_1 e^{-\lambda_1 t} + A_2 e^{-\Lambda t} \cos(\gamma_\mu B t + \phi) + A_{\text{bg}}, \quad (2)$$

where B was kept fixed at 4 mT for all temperatures where the oscillation was resolvable, and ϕ is a phase offset. Fig. S3(b) shows transverse relaxation rate Λ and oscillation amplitude A_2 (normalised by the total relaxation). The results of these fits (Fig. S3(b)) show peaks in relaxation rates and amplitudes indicative of phase transitions (although we note that they occur at temperatures slightly below those identified via AC susceptibility). This provides evidence for two phase transitions, supporting the claim that there are (at least) two different Zn-doping levels in the powder, and each of these has a different transition temperature.

* Electronic address: A.Stefancic@warwick.ac.uk

† Electronic address: tom.lancaster@durham.ac.uk

¹ A. A. Coelho, Bruker AXS, Karlsruhe, Germany (2012).

² D. R. Allan, H. Nowell, S. A. Barnett, M. R. Warren, A. Wilcox, J. Christensen, L. K. Saunders, A. Peach, M. T. Hooper, L. Zaja, et al., *Crystals* **7** (2017).

³ G. Winter, *Journal of Applied Crystallography* **43** (2010).

⁴ G. Winter, D. G. Waterman, J. M. Parkhurst, A. S. Brewster, R. J. Gildea, M. Gerstel, L. Fuentes-Montero, M. Vollmar, T. Michels-Clark, I. D. Young, et al., *Acta Crystallographica Section D* **74**, 85 (2018), URL <https://doi.org/10.1107/S2059798317017235>.

⁵ S. Bruker and B. A. SMART, *Acta Crystallogr., Sect. A: Found. Crystallogr* **64**, 112 (2008).

⁶ G. M. Sheldrick, *Acta Crystallographica Section A: Foundations and Advances* **71**, 3 (2015).

⁷ G. M. Sheldrick, *Acta Crystallographica Section C: Structural Chemistry* **71**, 3 (2015).

⁸ O. V. Dolomanov, L. J. Bourhis, R. J. Gildea, J. A. Howard, and H. Puschmann, *Journal of Applied Crystallography* **42**, 339 (2009).

⁹ H. Effenberger and F. Pertlik, *Monatshefte für Chemie/Chemical Monthly* **117**, 887 (1986).

¹⁰ H. Wu, T. Wei, K. Chandrasekhar, T. Chen, H. Berger, and H. Yang, *Scientific reports* **5**, 13579 (2015).

¹¹ S. Blundell, *Contemp. Phys.* **40**, 175 (1999).

Sample	a (Å)	V (Å ³)	% of Cu ₂ OSeO ₃	% of CuO	% of Zn ₂ SiO ₄	R_{wp}	R_{exp}	χ^2
0% Zn	8.923518(2)	710.572(0)	98.6(1)	1.45(1)	0.0	4.35	1.84	2.36
2% Zn	8.924835(4)	710.887(1)	83.1(1)	1.16(1)	0.0	4.14	1.94	2.14
	8.92718(4)	711.448(5)	11.8(1)					
	8.92962(4)	712.033(9)	3.9(1)					
4.1% Zn	8.925872(5)	711.135(1)	64.9(1)	1.3(1)	0.9(1)	3.98	1.87	2.13
	8.92883(1)	711.842(3)	26.5(1)					
	8.93135(3)	712.446(8)	6.3(1)					
6.4% Zn	8.926116(9)	711.193(2)	31.4(1)	1.0(1)	1.6(1)	4.03	1.79	2.25
	8.928525(7)	711.769(2)	53.2(1)					
	8.93142(1)	712.463(2)	12.5(1)					
7.9% Zn	8.926530(8)	711.292(2)	34.1(1)	1.4(1)	2.1(1)	4.70	1.91	2.46
	8.92928(1)	711.952(3)	37.6(1)					
	8.931560(9)	712.495(2)	24.8(1)					
10.5% Zn	8.927459(5)	711.514(1)	36.5(1)	3.0(1)	1.5(1)	4.16	1.86	2.23
	8.932180(3)	712.644(1)	59.0(1)					
13.4% Zn	8.92731(1)	711.480(3)	19.3(1)	4.9(1)	1.6(1)	3.96	1.93	2.05
	8.931850(2)	712.565(1)	74.1(1)					

TABLE S1: Lattice parameters values, quantities of phases present in the polycrystalline samples of (Cu_{1-x}Zn_x)OSeO₃ extracted from Rietveld refinements, along with qualities of fits.

Bonds	Pristine Cu ₂ OSeO ₃ (Å)	2.4% Zn (Å)	uncertainty (Å)	difference (Å)
Cu ^{II} – O1	1.9251(10)	1.9246(15)	0.00180	-0.0005
Cu ^{II} – O2	1.9675(10)	1.9680(17)	0.00197	+0.0005
Cu ^{II} – O3	2.0201(11)	2.0214(15)	0.00186	+0.0013
Cu ^{II} – O4	1.9728(10)	1.9761(14)	0.00172	+0.0033
Cu ^{II} – O4'	2.2847(10)	2.282(2)	0.00224	-0.0027
Cu ^I – O1	1.9225(10)	1.9265(15)	0.00180	+0.0040
Cu ^I – O2	1.9077(10)	1.9095(15)	0.00180	+0.0018
Cu ^I – O3	2.0851(11)	2.0829(16)	0.00194	-0.0022

TABLE S2: Bond lengths for single crystal samples, including overall uncertainty in the bond lengths.

Angles	Pristine Cu ₂ OSeO ₃ (Å)	2.4% Zn (Å)	uncertainty (Å)	difference (Å)
O1 – Cu ^{II} – O3	79.28(4)°	79.28(6)°	0.07	0.00
O1 – Cu ^{II} – O4	92.70(4)°	92.68(6)°	0.07	-0.02
O2 – Cu ^{II} – O3	100.59(4)°	100.68(6)°	0.07	+0.09
O2 – Cu ^{II} – O4	87.76(4)°	87.68(6)°	0.07	-0.08
O2 – Cu ^{II} – O4'	79.55(4)°	79.67(6)°	0.07	+0.12
O1 – Cu ^I – O3	77.74(4)°	77.72(6)°	0.07	-0.02
O2 – Cu ^I – O3	102.27(4)°	102.28(6)°	0.07	+0.01
O3 – Cu ^I – O3	115.61(2)°	115.60(3)°	0.04	-0.01

TABLE S3: Bond angles for single crystal samples, along with overall uncertainty in the bond angles.

Sample	0 %	2.9 %	4.1 %	6.4 %	7.9 %	10.5 %	13.4 %
T_c (K)	58.62(1)	51.6(2)	49.2(2)	48.7(1)	48.39(7)	47.97(3)	47.89(3)
		53.7(3)	52.10(8)	52.32(6)	51.61(7)	54.80(8)	54.3(1)
		57.33(2)	55.99(2)	55.45(5)	55.21(5)		
Weight	1.0	0.07(2)	0.090(9)	0.16(1)	0.26(1)	0.64(1)	0.80(1)
		0.06(2)	0.235(9)	0.43(1)	0.36(1)	0.35(2)	0.20(2)
		0.870(7)	0.675(8)	0.41(1)	0.38(1)		

TABLE S4: Ordering temperatures and the quantities of phases present in polycrystalline samples extracted from the gradient of $M - T$ magnetometry.

Substitution levels	0% Zn	0.5% Zn	1.8% Zn	2.4% Zn
T_c (K) in single crystals	58.30(2)	58.09(2)	56.96(2)	55.98(2)

TABLE S5: Ordering temperatures (T_c) observed in single crystals; obtained from $M - T$ magnetization.